IEEE Photonics Journal
An IEEE Photonics Society Publication

Open Access

Polarization-Selective Holographic Metasurface For Creating Cylindrical Vector Beams

Volume 11, Number 4, August 2019

Jiannong Chen
Qinfeng Xu
Jing Han

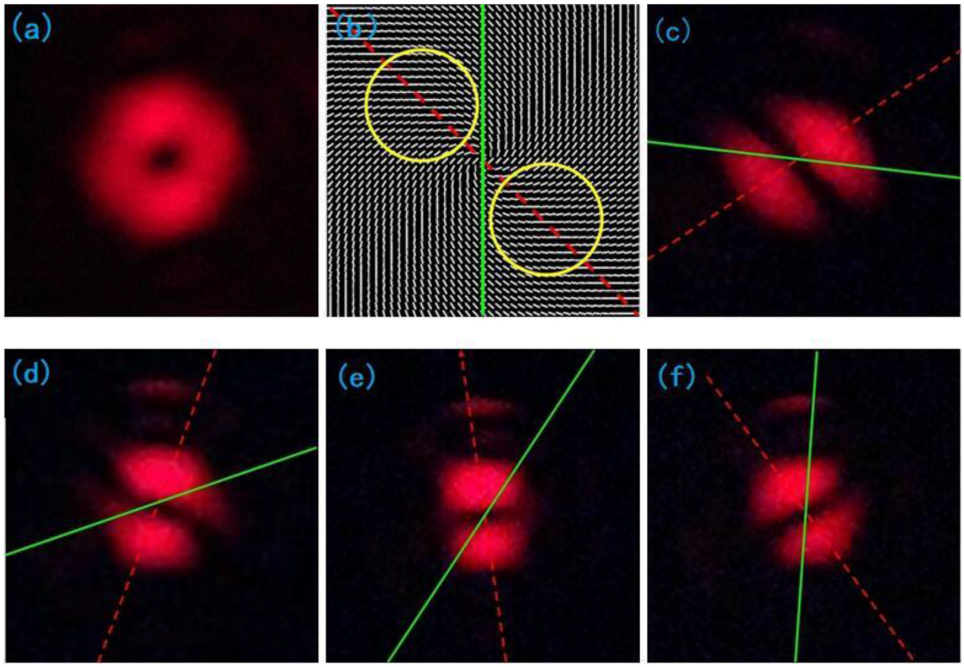

DOI: 10.1109/JPHOT.2019.2922218
1943-0655

IEEE photonics SOCIETY

IEEE

Polarization-Selective Holographic Metasurface For Creating Cylindrical Vector Beams

Jiannong Chen, Qinfeng Xu, and Jing Han

School of Physics and Optoelectronic Engineering, Ludong University, Yantai 264025, China

DOI:10.1109/JPHOT.2019.2922218

Manuscript received December 24, 2018; revised June 3, 2019; accepted June 6, 2019. Date of publication June 12, 2019; date of current version July 10, 2019. This work was supported in part by the National Natural Science Foundation of China (61307067), in part by the Shandong Natural Science Foundation (ZR2017MA035, ZR2019MF057, and ZR2019PF013), and in part by the Shandong Province Science and Technology Development Project (J18KA222). Corresponding author: Qinfeng Xu (e-mail: ldphysics2017@163.com).

Abstract: Generalized cylindrical vector beams (GCVB) are spatially polarization inhomogeneous. It could be considered as a combination of a radially polarized beam and an azimuthally polarized beam with different weighting factors. Here, we report a holographic metasurface patterned on a gold film layer for generating a GCVB. The nanostructure is a superposition of an individually oriented nanoslit array that determines the polarization distribution of the GCVB and a binary fork hologram that eliminates the additional Pancharatnam–Berry phase resulted from the circularly polarized incident plane beam. The behavior of a single nanoslit with specific parameters as a nanopolarizer and that of the overall holographic metasurface when illuminated by a circularly polarized plane beam are simulated and verified. A GCVB with plane wavefront and doughnut-shaped intensity distribution is experimentally produced using this holographic metasurface. The polarization state of the GCVB is also detected and confirmed.

Index Terms: Metasurfaces, cylindrical vector beams.

1. Introduction

The functions of conventional optical elements such as optical lens, polarizer, prism, and wave plate are realized by propagating light over a distance much longer than the operating wavelength. The substantial modulation of the amplitude, phase, or polarization is gradually accumulated during the propagation along the light path. Therefore, these devices usually have a large size and heavy weight which makes them unsuitable for fast-growing large-scale optoelectronic integrated circuits. With the development of nanofabrication technology, the study of metasurfaces capable of generating abrupt polarization, phase and amplitude modulation, has become a newly emerging field for constructing the compact, ultrathin flat optical components [1]–[4]. They are usually composed of arrays of subwavelength light scatterers with spatially varying geometric parameters. For example, scatters can be optical nanoantennas with different shapes, sizes or orientations. The size of a single cell in a scatter array and the spacing between adjacent cells are much smaller than the incident beam wavelength. Due to the subwavelength scale of a single cell in a scatter array, the dimensions of the overall component can usually be in the order of hundreds of micrometers or even less. Owing to

this feature of metasurfaces and the ability to engineer the local amplitude, phase, and polarization response with subwavelength resolution, metasurfaces form a very attractive research area. In this regard, a large number of devices and components have been reported so far [1], [3], [5].

Cylindrical vector beams with circularly symmetrical polarization, phase, and amplitude distribution in their cross-sections form an important family of beams, and include radially polarized beams, azimuthally polarized beams, and generalized cylindrical vector beams(GCVB) [6]. In fact, radially polarized beams and azimuthally polarized beams are special cases of GCVB. The GCVB can be expressed as a linear superposition of radially polarized beams and azimuthally polarized beams both of which are solutions of Maxwell's equations. They are spatially polarization-variant beams which are different from spatial polarization-homogeneous beams such as circularly polarized beams and linearly polarized beams. The cylindrically symmetric property of the polarization of cylindrical vector beams provides some special applications. For example, the focal spot size of a radially polarized beam can be much smaller than the diffraction limit of the focusing spot of spatially polarization-homogeneous beams [7], [8]. The applications such as laser processing, optical data storage, and fluorescent imaging can benefit from this tight focusing. The pure phase modulation of an azimuthally polarized beam can generate a superlong magnetized needle with a high aspect ratio in magnetic materials [9]. The light passing through plasmonic lenses constructed with concentric circular periodic metal slits are most efficiently coupled into surface plasmon polaritons when they are illuminated by radially polarized beams [10], [11].

Many generation methods of radially polarized beams and azimuthally polarized beams have been reported over the past decades [12]– [14]. In most of these methods, large optical beams are generated using bulky optical elements. Therefore they are not suitable for integrated photonic circuits. Based on the polarization-selective nature of nanoslits, some specially designed nanostructures which are patterned on a noble metal film or dielectric medium have been fabricated to generate a radially polarized beam or an azimuthally polarized beam when a circularly polarized beam impinges on the nanostructure [15]– [17]. In this study, we demonstrate the creation of GCVB with an ultrathin holographic metasurface composed of a square metal nanoslit array and a holographic nanostructure.

2. Scheme Details

The nanoslit patterned on the metal film serves as a nanoantenna when a light beam illuminates on it from the substrate side. The propagating surface plasmonic wave on the metal-air interface and the scattered radiating wave are both excited. The phase, amplitude, and polarization of both the waves strongly depend on the incident beam and the shape of the nanoslit. The surface plasmonic wave emitted from the nanoslit could be similar to the waves excited on the in-plane dipole on the interface [18], [19]. The polarization components of the electric field scattered from the nanoslit changes with the aspect ratio of length to width. The overall size of an individual nanoslit must be smaller than the wavelength of the incident beam in free space in order to form a desired wavefront according to Huygens' principle. Furthermore, as a single polarization-selective element, an individual nanoslit must also be capable of transmitting one polarization component of the incident beam while eliminating the orthogonal component with a high extinction ratio. Figs. 1(a) and (b) show the simulated intensity distributions of the x-polarized component and the y-polarized component with commercial FDTD solutions when the incident beam is a combination of an x-axis polarized plane beam and a y-axis polarized plane beam with equal intensity and the same phase. Fig. 1(c) is a three-dimensional model of a single nanoslit. The nanoslit is horizontally oriented with its length aligned along the x-axis. The intensity extinction ratio of the transmitted y-axis polarized component to the x-axis polarized component is estimated to be higher than 90.

With this specific nanoslit at hand, we now describe the architecture for constructing the holographic metasurface. We assume that the metasurface area is a big square and it is equally divided into a M$\times$M small square unit array as shown in Fig. 2. The side of each identical small square is equal to the length of the nanoslit which is 400 nm. In each of the M$\times$M identical small square units there is a nanoslit and the center of each small square unit has the same position as that of the

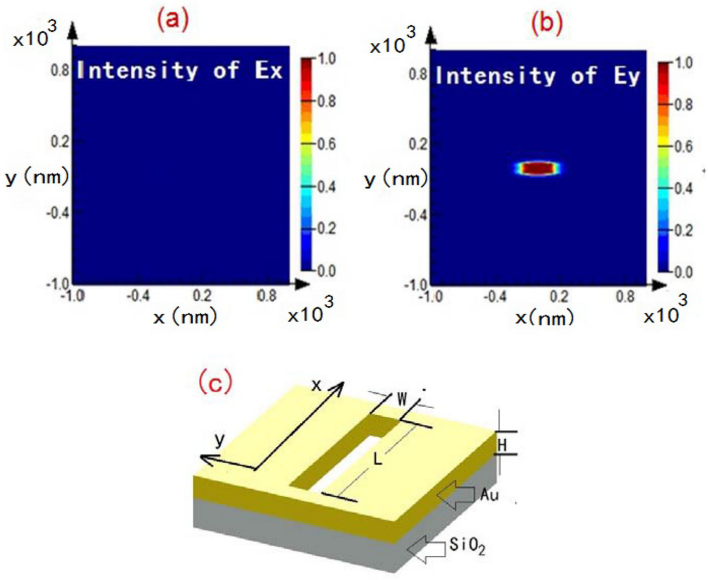

Fig. 1. (a) and (b) Comparison of the intensities of two orthogonally polarized components transmitted from a nanoslit when the incident beam is a combination of an x-axis polarized plane beam and a y-axis polarized plane beam with equal intensities and the nanoslit is horizontally oriented with the length aligned along the x-axis. (c) the three dimensional model of a nanoslit etched into the gold film on the SiO2 substrate. the width, the length and the height of the nanoslit are $W = 80$ nm, $L = 400$ nm and $H = 150$ nm.

rectangular center of the nanoslit. The orientation of the nanoslit can be determined from the azimuthal angle ϕ with respect to the x-axis in x-o-y coordinate system. Here the angle ψ is called the general cylindrical angle. As illustrated in Fig. 2, ψ is measured with respect to the radial electric vector E_r. E_a denotes an azimuthal electric vector and E_g denotes the general electric vector. When $\psi = 0$, the general electric vector reduces to a radial electric vector; when $\psi = 90^\circ$, it reduces to an azimuthal electric vector. It is easily seen that $E_g = E_r + E_a$, $|E_r| = |E_g| \cos\psi$, $|E_a| = |E_g| \sin\psi$. Thus we can deduce that GCVB can be taken as the vector superposition of a radially polarized beam and an azimuthally polarized beam with different weighting factors. Conversely, the radially polarized beam or azimuthally polarized beam can be taken as a specific case of GCVB. Here E_g is perpendicular to the nanoslit because only the electric component of the incident beam perpendicular to the nanoslit can pass through the nanoslit as demonstrated in Fig. 1.

The inset in Fig. 2 shows an enlarged small square unit of the metasurface area in the i-th row and j-th column. Here i = 1,2,. . . M, j = 1,2,. . . M. In our design, $\psi = 45^\circ$ is a constant in each of the M×M small square units. The nanoslit array will appear as shown in Fig. 3(a). When the incident beam is a circularly polarized beam, the transmitted beam will have an additional vortex phase with a polarization perpendicular to the nanoslit in each small square unit. It is called Pancharatnam-Berry phase [20]. The value of the Pancharatnam-Berry phase φ is equal to 2ϕ of the rotation with respect to the x-axis as illustrated in Fig. 2. The phase distribution in the X-O-Y coordinate system is the same as the vortex phase expressed as $\exp(i\varphi)$.

The nanoslit, as a single linear polarizer, has the Jones vector in the format of matrix as following [15], [21]:

$$M = \begin{pmatrix} \cos^2\varphi & \sin\varphi\cos\varphi \\ \sin\varphi\cos\varphi & \sin^2\varphi \end{pmatrix} \quad (1)$$

Where φ is the angle between the polarization direction of electric vector and the x axis. When a circularly polarized plane beam is incident on the nanoslit, the light transmitted through the nanoslit

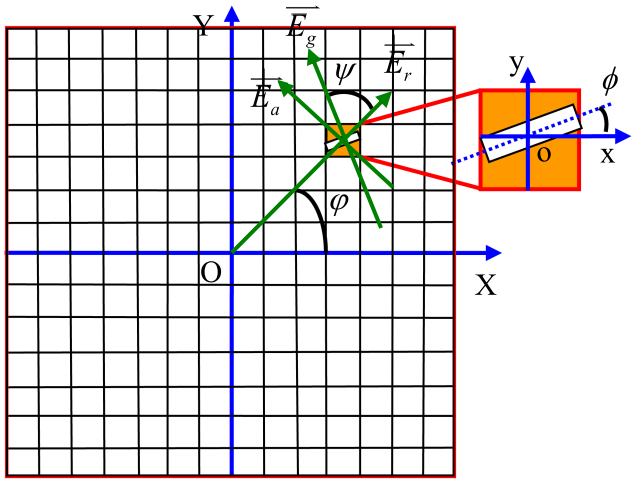

Fig. 2. Schematic of the architecture for constructing the holographic metasurface. $\vec{E}_a$ denotes an azimuthal electric vector; $\vec{E}_r$ denotes a radial electric vector; $\vec{E}_g$ denotes the general electric vector. The inset is an enlarged small square unit of the metasurface area. ϕ is the azimuthal angle in the X-O-Y coordinate system. ψ is the general cylindrical angle. φ is the rotation angle of the individual nanoslit measured with respect to x-axis in x-o-y coordinate system.

can be described as

$$E = \exp(i \pm \varphi) \begin{pmatrix} \cos\varphi \\ \sin\varphi \end{pmatrix} \tag{2}$$

As is seen that a Pancharatnam-Berry phase or the vortex phase is induced. The positive and nagetive sign in Eq. (2) correspond to the right-handed and left-handed circularly polarized beam, respectively. Therefore the metasurface as shown in Fig. 3(a) which is illuminated with a circularly polarized beam will produce a general cylindrical vortex vector beam(GCVVB).

To eliminate the additional vortex phase, it is desirable to produce another vortex phase with opposite topological charge using another nanostructure simultaneously. This nanostructure must combine with the structure of the nanoslit array otherwise the additional vortex phase cannot be compensated or cancelled. Here, the nanostructured hologram is the best choice. According to holography theory, the object beam must be a vortex beam with opposite topological charge of the Pancharatnam-Berry phase. Here the reference beams can be a circularly polarized plane beam. The hologram is the interferogram between the reference beam and vortex beam. It is a fork hologram as displayed in Fig. 3(b). The size of the fringe pattern strongly depends on the angle between the two interfering beams. It also inevitably determines the separation degree of different diffracting orders. We carefully designed hologram and the period of the fringe pattern is around 1.2 μm. Fig. 3(c) shows the superimposed nanostructure of Fig. 3(a) and Fig. 3(b). The gray level in Fig. 3(c) is continuous. It is not practicable for modern fabrication technologies such as electron beam (EB) and focused ion beam (FIB). It is necessary to simplify the nanostructure with the continuous gray level into an appropriate nanostructure with binary gray level. Fig. 3(d) shows the binary nanostructure after simplification.

3. Simulation and Experimental Demonstration

To ensure the feasibility of the holographic metasurface architecture, we imported the superimposed nanostructure into a simulation model constructed using the Lumerical software for Finite-Difference in Time-Domain (FDTD). The size of the nanostructure is 30 μm $\times$ 30 μm $\times$ 150 nm and the computation volume is 30 μm $\times$ 30 μm $\times$ 170 nm. The substrate we used in calculation is SiO_2

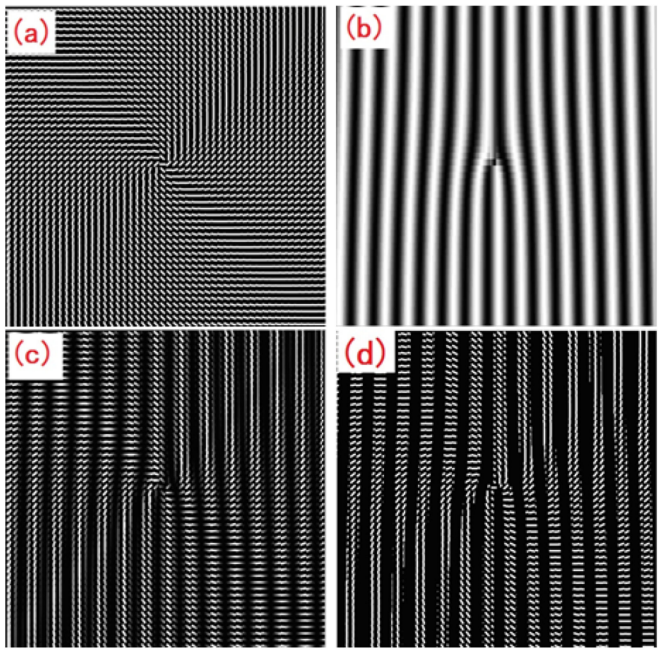

Fig. 3. Nanostructure for generating cylindrical vector beams. (a) the properly rotated nanoslit array; (b) the interferogram produced by interfering the vortex phase beam with the reference plane beam; (c) superimposed nanostructure with continuous gray level; (d) superimposed nanostructure with binary gray level.

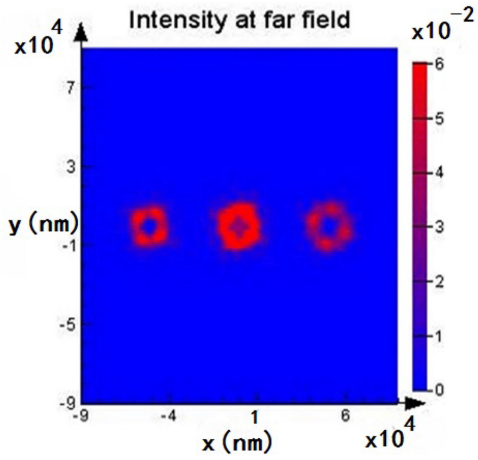

Fig. 4. Simulated electric intensity distribution in the far field when the superimposed nanostructure is illuminated with a circularly polarized plane beam. The doughnut-shaped intensity distribution on the two sides are positive first order diffraction and negative first order diffraction.

on which a gold film was deposited with the thickness of 150 nm. The data of the gold film and SiO_2 substrate are obtained from the study by Palik. The white color shown in Fig. 3(d) is etched away when it is overlapped with the gold film in the three-dimensional model while the black color represents the remaining gold film. The incident beam is a circularly polarized plane wave. The electric field monitor is kept parallel to the interface between the gold film and air, and is 10 nm away from the gold film. We calculated the electric field intensity 100 um away from the near field monitor by script command “farfieldexact3D”. Fig. 4 shows the three diffracting orders. In the

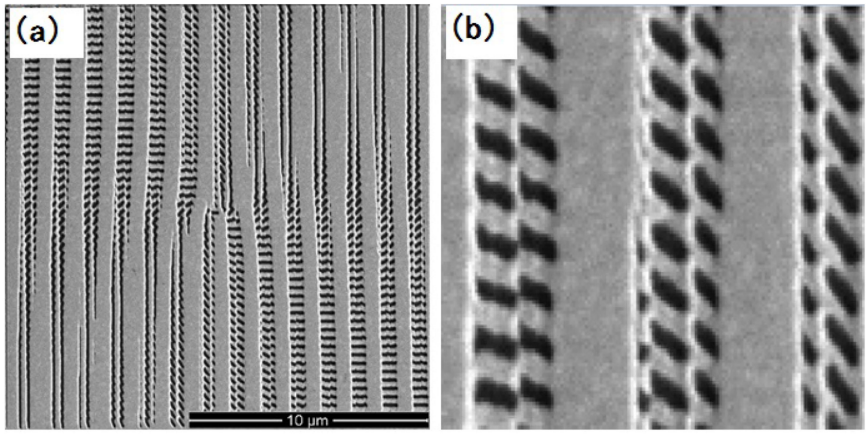

Fig. 5. (a) The image of a small sample obtained by the scanning electron microscope(SEM). The size is around 16 μm $\times$ 16 μm; (b) Local magnified SEM image.

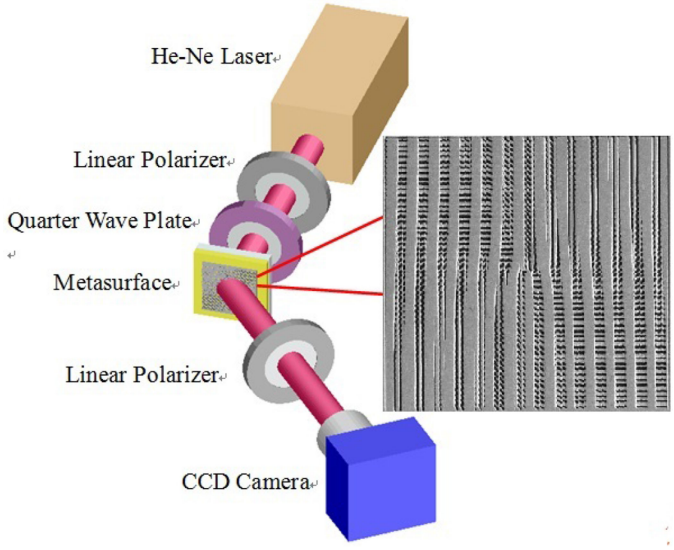

Fig. 6. Experiment setup for observing the produced GCVB.

positive first order, we obtained the doughnut-shaped intensity distribution with plane wave front. The defect and the deviation from the ideal doughnut shape may have arisen from the imported nanostructure error and the relatively big mesh gap in the calculation. Fundamentally, the doughnut-shaped intensity distribution is resulted from the rotational symmetric feature of the polarization of GCVB because the electric field vectors on the axis and its vicinity will cancel each other and results in the zero intensity on the axis.

For the fabrication of the sample, a 10 nm thick chromium film and a layer of gold film with a thickness of 150 nm were successively deposited on the substrate using electron beam evaporation method. The binary superimposed nanostructure shown in Fig. 3(d) was saved in the bitmap format in advance. It was then imported into the focusing ion beam machine (Helios Nanolab 600, FEI) using the built-in controlling software. The fabricated sample has the transverse size of 50 μm $\times$50 μm. Fig. 5(a) displayed the scanning electron microscope(SEM) image of another fabricated small holographic metasurface. The scale bar at the right-bottom corner is 10 μm. Fig. 5(b) provided a local magnified SEM picture of the fabricated nanostructure. Fig. 6 shows the

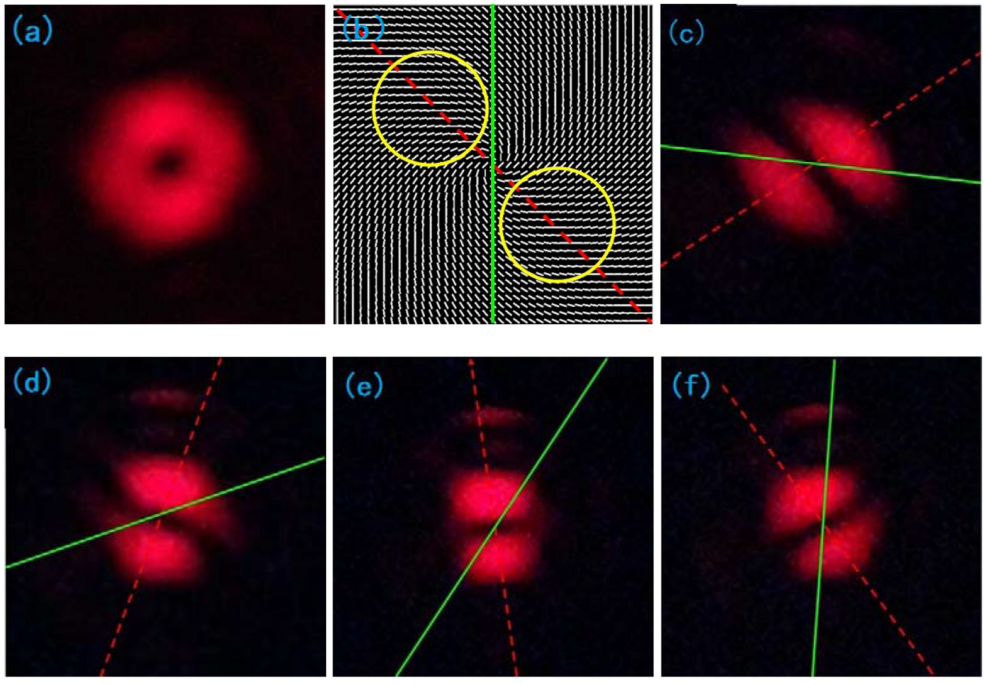

Fig. 7. Detection of the polarization orientation of the GCVB. (a) shows a measured intensity distribution captured by the camera when the linear polarizer just before it is removed; (b) illustrates the relation between the transmittance axis of the linear polarizer placed just before (green solid line) and the circled area (yellow line) in which the nanoslits are almost perpendicular to the transmittance axis of the linear polarizer. Red dashed line connects the two circle centers. (c), (d), (e), and (f) demonstrates that the two lobes of intensity distribution captured by the CCD camera rotates following the change of orientation of the linear polarizer.

experimental setup for producing, observing and detecting GCVB. The He-Ne laser with a wavelength of 633 nm is converted into a circularly polarized beam by passing it through a linear polarizer and a quarter wave plate. Then, the circularly polarized beam is directly incident on the holographic metasurface. On the optical path of the first order of diffraction, a linear polarizer which acts as a polarization filter and a CCD camera which is far away enough to separate the first diffraction order and zero order were placed. Fig. 7(a) shows a measured intensity distribution captured by the camera when the linear polarizer just before it is removed. It has a doughnut-shaped distribution which agrees well with the result of the FDTD simulation as demonstrated in Fig. 4.

In order to verify that the spatially polarization distribution of the experimentally produced GCVB is as the one theoretically predicted, we insert a linear polarizer into the optical path between the holographic metasurface sample and the CCD camera, and then rotate the linear polarizer. The intensity distributions detected by the camera change with the rotation of the linear polarizer. Fig. 7(b) shows the theoretical relation between the transmittance axis of the linear polarizer (solid green line) and the line (red dashed line) connecting the two lobes (two yellow circled areas). In the yellow circled areas, the orientation of the nanoslits is almost perpendicular to the transmittance axis of the linear polarizer. Therefore the incident light impinging on these areas can pass through the linear polarizer just before the CCD camera. Fig. 7(c), Fig. 7(d), Fig. 7(e) and Fig. 7(f) demonstrate that the red dashed line connecting the two transmitted lobes rotates with changes in the transmittance axis (solid green line) of the linear polarizer. In each of the subfigures, the angle between the solid green line and the red dashed line is always equal to designed angle $\psi = 45^\circ$ (as described above, it is termed the general cylindrical angle).

Fig. 8 is the simulated transmittance spectrum of the designed structure we used in the experiment. As is shown, the nanostructure has a maximum transmittance at the wavelength of around

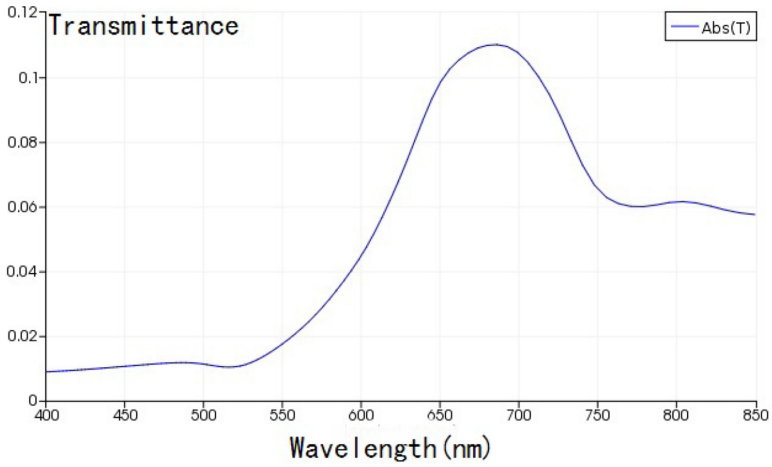

Fig. 8. The transmittance spectrum of the fabricated nanostructure in the experiment.

680 nm. The full width at half Maximum is approximately 230 nm. It exhibits a broadband feature. However, they mostly fall on the red and near infrared region, some frequently-used wavelengths in the visible region such as 532 nm, are not suitable for the designed structure. For further investigation, it is necessary to specifically design the nanostructure using the proposed method for lasers emitting lights with short visible wavelength.

4. Conclusion

We have proposed a metasurface architecture for producing GCVB when the incident beam is a circularly polarized plane beam. The metasurface is composed of an appropriately rotated nanoslit array which is designed to create polarization distribution of the GCVB and a superimposed interferogram which is designed to compensate or cancel the vortex phase induced when the incident circularly polarized beam impinges on the rotationally symmetric nanoslit array. We theoretically simulated and verified the polarization-selective property of an individual nanoslit with an optimized aspect ratio and the capability of the holographic metasurface for producing GCVB with a plane wave front. We also experimentally demonstrated and detected the GCVB and its spatial polarization distribution which agrees well with the design and theoretical simulation. Although the general cylindrical angle is 45° in our simulation and experiment, it can be any value between 0° and 90°. It means that we can produce arbitrary GCVB which can be taken as a superimposition of a radially polarized beam and an azimuthally polarized beam with different weighting factors. Many features of the GCVB are similar to these of the well studied radially polarized beam and azimuthally polarized beam. The production of GCVB with holographic metasurface may provide many potential applications.

References

[1] A. V. Kildishev, A. Boltasseva, and V. M. Shalaev, "Planar photonics with metasurfaces," *Science*, vol. 339, 2012, Art. no. 1232009.
[2] N. Yu, P. Genevet, F. Aieta, M. A. Kats, and R. Blanchard, "Flat optics: Controlling wavefronts with optical antenna metasurfaces," *IEEE J. Sel. Top. Quantum Electron.*, vol. 19, no. 3, May/Jun. 2013, Art. no. 4700423.
[3] Z. Wei, Y. Cao, X. Su, Z. Gong, Y. Long, and H. Li, "Highly efficient beam steering with a transparent metasurface," *Opt. Exp.*, vol. 21, no. 9, pp. 10739–10745, 2013.
[4] N. Yu, F. Aieta, P. Genevet, M. A. Kats, Z. Gaburro, F. Capasso, "A broadband background-free quarter-wave plate based on plasmonic metasurfaces," *Nano Lett.*, vol. 12, no. 12, pp. 6328–6333, 2012.

[5] A. Pors, M. G. Nielsen, R. L. Eriksen, and S. I. Bozhevolnyi, "Broadband focusing flat mirrors based on plasmonic gradient metasurfaces," *Nano Lett.*, vol. 13, no. 2, pp. 829−834, 2013.
[6] Q. Zhan, "Cylindrical vector beams: From mathematical concepts to applications," *Adv. Opt. Photon.*, vol. 1, no. 1, pp. 1–57, 2009.
[7] R. Dorn, S. Qubis, and G. Leuchs, "Sharper focus for a radially polarized light beam," *Phys. Rev. Lett.*, vol. 91, no. 23, 2003, Art. no. 233901.
[8] H. Wang, L. Shi, B. Lukyanchuk, C. Sheppard, and C. T. Chong, "Creation of a needle of longitudinally polarized light in vacuum using binary optics," *Nature Photon.*, vol. 2, no. 8, pp. 501–505, 2008.
[9] S. Wang, X. Li, J. Zhou, and M. Gu, "Ultralong pure longitudinal magnetization needle induced by annular vortex binary optics," *Opt. Lett.*, vol. 39, no. 17, pp. 5022–5025, 2014.
[10] A. Yanai and U. Levy, "Plasmonic focusing with a coaxial structure illuminated by radially polarized light," *Opt Exp.*, vol. 17, no. 2, pp. 924–932, 2009.
[11] W. Chen, D. C. Abeysinghe, R. L. Nelson, and Q. Zhan, "Plasmonic lens made of multiple concentric metallic rings under radially polarized illumination," *Nano Lett.*, vol. 9, no. 12, pp. 4320–4325, 2009.
[12] J. F. Bisson, J. Li, K. Ueda, and Y. Senatsky, "Radially polarized ring and arc beams of a neodymium laser with an intra-cavity axicon," *Opt. Exp.*, vol. 14, no. 8, pp. 3304–3311, 2006.
[13] Y. Kozawa and S. Sato, "Generation of a radially polarized laser beam by use of a conical brewster prism," *Opt. Lett.*, vol. 30, no. 22, pp. 3063–3065, 2005.
[14] X. Wang, J. Ding, W. J. Ni, C. S. Guo, and H. Wang, "Generation of arbitrary vector beams with a spatial light modulator and a common path interferometric arrangement," *Opt. Lett.*, vol. 32, no. 24, pp. 3549–3551, 2007.
[15] J. Wen, H. Feng, J. Chen, K. Wang, Y. Lv, Y. Zhong, and D. Zhang, "Plasmonic holographic metasurfaces for generation of vector optical beams," *IEEE Photon. J.*, vol. 9, no. 1, Feb. 2017, Art. no. 4600108.
[16] F. Wang, M. Xiao, K. Sun, and Q. Wei, "Generation of radially and azimuthally polarized light by optical transmission through concentric circular nanoslits in Ag films," *Opt. Exp.*, vol. 18, no. 1, pp. 63–71, 2009.
[17] P. Yu *et al.*, "Generation of vector beams with arbitrary spatial variation of phase and linear polarization using plasmonic metasurfaces," *Opt. Lett.*, vol. 40, no. 14, pp. 3229–3232, 2015.
[18] T. Tanemura, K. C. Balram, D. S. Ly-Gagnon, P. Wahl, J. S. White, and M. L. Brongersma, "Multiple-wavelength focusing of surface plasmons with a nonperiodic nanoslit coupler," *Nano Lett.*, vol. 11, no. 7, pp. 2693–2698, 2011.
[19] J. Lin *et al.*, "Polarization-controlled tunable directional coupling of surface plasmon polaritons," *Science*, vol. 340, no. 6130, pp. 331–334, 2013.
[20] D. Lin, P. Fan, E. Hasman, and M. L. Brongersma, "Dielectric gradient metasurface optical elements," *Science*, vol. 345, no. 6194, pp. 298–302, 2014.
[21] M. Kang, J. Chen, X. L. Wang, and H. T. Wang, "Twisted vector field from an inhomogeneous and anisotropic metamaterial," *J. Opt. Soc. Amer. B*, vol. 29, no. 4, pp. 572–576, 2012.
[22] J. Lin, P. Genevet, M. A. Kats, N. Antoniou, and F. Capasso, "Nanostructured holograms for broadband manipulation of vector beams," *Nano. Lett.* vol. 13, pp. 4269–4274, 2013.